

Fermionic Order by Disorder in a van der Waals Antiferromagnet

R. Okuma^{1*}, D. Ueta^{1*}, S. Kuniyoshi^{1,2*}, Y. Fujisawa¹, B. Smith¹, C. H. Hsu^{1,3}, Y. Inagaki⁴,
W. Si⁴, T. Kawae⁴, H. Lin⁵, F. C. Chuang^{3,6}, T. Masuda⁷, R. Kobayashi², Y. Okada¹
mail: yoshinori.okada@oist.jp

¹*Quantum Materials Science Unit, Okinawa Institute of Science and Technology (OIST),
Okinawa 904-0495, Japan*

²*Faculty of Science, University of the Ryukyus, Nishihara, Okinawa 903-0213, Japan*

³*Department of Physics, National Sun Yat-sen University, Kaohsiung 80424, Taiwan*

⁴*Department of Applied Quantum Physics, Kyushu University, Fukuoka 819-0395, Japan*

⁵*Institute of Physics, Academia Sinica, Taipei, Taiwan*

⁶*Physics Division, the National Center for Theoretical Sciences, Hsinchu, 30013, Taiwan*

⁷*Institute for Solid State Physics (ISSP), The University of Tokyo, Kashiwa, Chiba 277-8581, Japan*

Abstract

CeTe₃ is a unique platform to investigate the itinerant magnetism in a van der Waals (vdW) coupled metal. Despite chemical pressure being a promising route to boost quantum fluctuation in this system, a systematic study on the chemical pressure effect on Ce³⁺(4f¹) states is absent. Here, we report on the successful growth of a series of Se doped single crystals of CeTe₃. We found a fluctuation driven exotic magnetic rotation from the usual easy-axis ordering to an unusual hard-axis ordering. Unlike in localized magnetic systems, near-critical magnetism can increase itinerancy hand-in-hand with enhancing fluctuation of magnetism. Thus, seemingly unstable hard-axis ordering emerges through kinetic energy gain, with the self-consistent observation of enhanced magnetic fluctuation (disorder). As far as we recognize, this order-by-disorder process in fermionic system is observed for the first time within vdW materials. Our finding opens a unique experimental platform for direct visualization of the rich quasiparticle Fermi surface deformation associated with the Fermionic order-by-disorder process. Also, the search for emergent exotic phases by further tuning of quantum fluctuation is suggested as a promising future challenge.

Introduction

In the search for interesting metallic states in quantum materials, controlling magnetic orientation, fluctuations, and their interaction with conduction electrons has been of utmost importance. Consequent exotic phases are rich, ranging from unconventional superconductivity^{1,2,3,4} to giant magneto-transport effects, including metal-to-insulator transition⁵, magnetically driven 2D confinement⁶, and exotic Hall effects^{7,8,9,10,11,12,13,14}. One of the most important recent challenges within this field is exploring the exotic magnetic metallic state in van der Waals (vdW) coupled materials^{15,16,17,18,19,20,21}. A missing but crucial component in this challenge is establishing various approaches to controlling the interaction between magnetism and conduction and the mechanism by which they operate.

CeTe₃ provides a unique platform to investigate the itinerant magnetism in a van der Waals (vdW) coupled metal^{22,23,24}. The crystal structure of CeTe₃ features a square net of Te^{0.5-} and rock-salt type layer of Ce³⁺ and Te²⁻ (**Fig. 1a**), combined to realize a highly two-dimensional vdW motif^{21, 25}. The conduction band mainly originates from the Te^{0.5-} square net; Ce³⁺ is responsible for magnetism. Strong nesting of the Fermi surface derived from the square net Te sheet causes a 1D-like charge density wave (CDW) transition below 400 K^{26,27,28,29,30}, whose temperature scale is well separated from the much lower magnetic transition temperature. Based on previous studies^{23,31}, the magnetic moment of CeTe₃ can be described as a pseudo spin 1/2 system with strongly easy-plane (XY) character, and long range antiferromagnetic order along the easy-plane is observed below 1.3 K.

Recently, CeSeTe₂ has been identified as a compound closely related to CeTe₃. In CeSeTe₂, Se²⁻ selectively substitutes into Te²⁻ sites in CeTe₃^{32,33}. Consistent with the chemical and structural similarity of CeSeTe₂ to CeTe₃ (**Fig. 1a**), a CDW transition and strongly easy-plane like magnetism in the paramagnetic regime are observed in both materials³¹. In CeSeTe₂ however, the reported magnetism in the ordered state is consistent with a collinear structure pointing in the out-of-plane direction³¹, which is strongly unfavorable in the paramagnetic state. Thus, by defining the magnetic hard and easy axis/plane of the system based on its paramagnetic state, surprising *hard-axis ordering* is suggested to emerge in CeSeTe₂ below the antiferromagnetic phase transition. Despite this unusual direction of magnetic moment in the ordered state, no detailed measurements have been performed so far to elucidate the underlying mechanism.

To understand the origin of this peculiar hard-axis ordering, here we studied the effect of Se doping systematically through magnetization and heat capacity measurement of Ce(Se_xTe_{1-x})Te₂. We confirmed that addition of Se applies chemical pressure to Ce³⁺, which results in exotic reorientation

of the magnetic moment through enhanced quantum fluctuation. In this report, we present that the presence of hard-axis ordering is representative of the fermionic order by disorder process, in which a seemingly unstable direction is stabilized through itinerant energy gain.

Results

Crystal growth of $\text{Ce}(\text{Se}_x\text{Te}_{1-x})\text{Te}_2$. Single crystals of $\text{Ce}(\text{Se}_x\text{Te}_{1-x})\text{Te}_2$ were grown via the flux method (See method for detail). This formula represents that Se^{2-} selectively replaces Te^{2-} in the magnetic blocking layer (**Fig. 1a**). Thus, Se^{2-} doping connects the two isostructural systems $\text{Ce}^{3+}(\text{Te}^{2-})(\text{Te}^{0.5-})_2$ and $\text{Ce}^{3+}(\text{Se}^{2-})(\text{Te}^{0.5-})_2$. Since the ionic radii of Se^{2-} and Te^{2-} are 1.98 Å and 2.21 Å, respectively³⁴, systematic control of chemical pressure becomes possible in $\text{Ce}(\text{Se}_x\text{Te}_{1-x})\text{Te}_2$ through variation of the doping ratio. The single crystals of $\text{Ce}(\text{Se}_x\text{Te}_{1-x})\text{Te}_2$ present a plate-like morphology with shiny surfaces, reflecting the vdW coupling nature in our system (**Fig. 1a**). **Fig. 1b** shows the doping evolution of the X-ray diffraction (XRD) pattern around the (080) peak. **Fig. 1c** shows the relationship of the lattice constant along the out-of-plane b axis and the Se/Te ratio x as determined by XRD and energy dispersive X-ray spectrometry (EDX), respectively. As predicted by Vegard's law, the monotonic linear behavior of the shrinkage of lattice constant with doping suggests the systematic replacement of smaller ionic radii Se^{2-} into the larger ionic radii Te^{2-} sites. Similar monotonic shrinkage of the out of plane lattice constant by doping with elements with smaller ionic radii is also seen in another vdW misfit compounds such as Bi-based cuprates³⁴. In this study, using the obtained linear function, we calculated x from the out-of-plane lattice constant of the crystal flakes used for heat capacity and magnetic measurements.

Magnetic order in CeSeTe_2 and CeTe_3 . We first present a significant difference in the magnetism and heat capacity behavior of CeTe_3 (**Fig. 2a**) and CeSeTe_2 (**Fig. 2b**), despite the common easy-plane feature in the paramagnetic regime. In **Fig. 2a and b**, magnetic susceptibility $\chi(T)$ and heat capacity $C(T)$ are shown on the left and right axes, respectively. For the parent compound CeTe_3 , we see two characteristic antiferromagnetism related transition temperatures T_{N1} and T_{N2} . Only a broad peak is observed in $C(T)$ around T_{N1} while around T_{N2} a sharp peak in $C(T)$ accompanies stronger suppression of $\chi(T)$ along the in-plane (blue and red curves) than the out-of-plane (green curve) direction. On the other hand, the doped system CeSeTe_2 features a single antiferromagnetic transition with a sharp peak at T_{N3} in $C(T)$ that accompanies stronger suppression of $\chi(T)$ along the out-of-plane (green curve) than the in-plane (blue and red curves) directions. Therefore, at the lowest temperature, the Néel vector points along the easy plane in CeTe_3 , whereas it points along the hard axis in CeSeTe_2 . This striking contrast is also evident from the suppression of susceptibility and spin flip and flop transitions (**Fig. 2c and 2d**) since they should appear along the Néel vector. **Fig. 2e** is the

experimentally determined magnetic hard axis and easy plane together with crystal axes. These directions are the same for all samples shown in this study.

Quasi two-dimensional magnetism of CeSeTe₂ and CeTe₃. The ordering phenomena in Ce(Se_xTe_{1-x})Te₂ based on localized spin picture are briefly discussed before we emphasize the importance of itinerancy. The magnetism of CeTe₃ and CeSeTe₂ is supposed to originate from highly two-dimensional interactions with XY-like and Ising-like anisotropy, respectively. In CeTe₃, the successive phase transitions associated with T_{N1} and T_{N2} are reminiscent of the 2D XY model perturbed by weak in-plane anisotropy³⁵. While two-dimensional XY-like interactions can support only quasi long-range order at a finite temperature, genuine long-range order can appear by nearly four-fold symmetric anisotropies at a lower temperature. This picture is presumably captured by the broad and sharp peaks T_{N1} and T_{N2} , respectively. In contrast, Ising-type long-range-order in CeSeTe₂ can appear by breaking discrete Ising symmetry; here in-plane anisotropy plays no role in the magnetic ordering and a single transition has been observed. The abrupt suppression of $\chi(T)$ also reflects on the stability of the Ising-like collinear order. It should be noted that the observed collinear magnetism suggests that the Dzyaloshinski-Moriya (DM) interaction, which favors noncollinear spin arrangement regardless of anisotropy of the g factor, should play a minor role in the emergence of hard axis magnetic order. At this stage, it remains unclear why the effective interaction becomes Ising-like by doping even though the paramagnetic susceptibility remains XY-like. As we discuss hereafter, beyond the localized magnetic picture, kinetic energy gain plays a crucial role in explaining an essential part of our experimental observation.

Magnetic fluctuation of Ce(Se_xTe_{1-x})Te₂. If the ordering direction of CeSeTe₂ is actually unfavorable, we should observe self-consistent consequences of enlarged quantum fluctuation. To check this, we investigated the systematic doping dependence of the magnetic fluctuation of Ce(Se_xTe_{1-x})Te₂. 4f-electron derived entropy $S(T)$ is estimated and plotted in **Fig. 3a-f** (right axis) based on the formula

$$S(T) = \int_0^T \frac{C_f}{T} dT$$
. Here, $C_f(T)$ is the heat capacity from the 4f electron contribution (See method for detail). We further calculate magnetic entropy S_m for $S(T_{N1})$ and $S(T_{N3})$ as $x < 0.54$ and $x > 0.54$, respectively. Based on a fully localized picture, S_m should asymptotically approach $R \ln 2$ ($\sim 5.76 \text{ JK}^{-1} \text{ mol}^{-1}$). This value is simply derived from the ground state doublet of Ce³⁺ ions under the crystalline electric field. Thus, $1 - S_m/R \ln 2$ can be taken as the measure of the strength of magnetic fluctuation for a given magnetic order.

Evolution of magnetic fluctuation by doping. By constructing a phase diagram, a correlation exists

between enhanced magnetic fluctuation and emergent hard-axis moment. **Fig. 4a** represents the phase diagram with three characteristic temperatures (left axis) together with $1-S_m/R\ln 2$ (right axis). With increasing doping x , T_{N1} and T_{N2} are systematically decreased for $x < 0.54$. Above $x = 0.54$, we see only one transition temperature T_{N3} . Therefore, combining magnetic measurements for CeTe_3 (**Fig. 2a**) and CeSeTe_2 (**Fig. 2b**), a first-order magnetic transition is expected to exist near $x = 0.54$, across which the direction of magnetic moment abruptly changes from the easy plane to the hard axis. The enhancement of $1-S_m/R\ln 2$ towards the first-order transition point is partly due to the chemical disorder effect since chemical entropy naturally reaches a maximum at $x = 0.5$ in our alloyed system. As a consequence, chemical disorder may contribute to a slight increase in $1-S_m/R\ln 2$ with doping levels above $x = 0.54$ (**Fig. 4a**). However, we emphasize that the values $1-S_m/R\ln 2$ for two nearly stoichiometric samples with $x = 0$ and $x = 0.96$ are 0.25 and 0.36, respectively. Based on these values, the magnetic fluctuation of stoichiometric CeSeTe_2 is expected to be ~ 1.4 times larger than that of the parent compound CeTe_3 . Therefore, the key feature to be captured in the phase diagram is an emergent hard-axis moment with a monotonic enhancement of magnetic fluctuation.

Discussion

We propose the possible mechanism leading to emergent hard axis ordering in terms of fermionic order by disorder in itinerant systems^{36,37}. Our observation is that the change in chemical pressure enhanced the magnetic quantum fluctuation and altered the direction of Néel vector to the apparent “hard axis”. This implies that magnetic quantum fluctuation itself drives the hard-axis ordering as in the case of “order by disorder” in frustrated magnets³⁸. The relevant quantum fluctuation is unlikely to be Kondo screening in our case because a similar magnitude of saturated magnetic moment along the easy-axis with doping was observed experimentally (**Fig. 2c** and **d**). Instead, we propose that the enhanced magnetic fluctuation is a spin-wave excitation, which is the primary fluctuation from the magnetically ordered state. An important point to note is that the spin-wave excitation is a transverse fluctuation. Since the transverse direction from the hard axis is on the easy plane, hard-axis order can fluctuate more easily than easy-plane order. We surmise that the hard-axis order becomes favorable when chemical pressure further enhances quantum fluctuation of localized spin through Kondo coupling.

Compared to localized frustrated magnets, fermionic order by disorder requires kinetic energy gain of electrons in addition to transverse spin fluctuation (**Fig. 4b**). Such physics is directly captured by investigating electronic quasiparticle band deformation to lower the total energy of the system. This concept is consistent with the Fermionic order-by-disorder process, as predicted theoretically^{36,37}. Regardless of theoretical proposals, however, experimental direct visualization of quasi-particle band

deformation has been missing due to the lack of proper materials to investigate with high resolution. Compared with materials in existing studies such as YbRh_2Si_2 , YbNi_4P_2 , and $\text{CeT}_2\text{Al}_{10}$ ($T = \text{Ru, Os}$)^{39,40,41,42,43,44,45} the intrinsically cleavable nature and simple composite structure of our vdW material offers an excellent platform for unveiling rich quasiparticle band deformation using surface sensitive spectroscopies with changing external magnetic field, its orientation and temperature. In addition, inherent applicability of advanced exfoliation techniques⁴⁶ will further enrich future challenges in searching for novel quantum phenomena.

In summary, we show magnetic fluctuation driven unusual magnetic rotation from the usual easy plane to unusual hard axis moment across the magnetic phase transition. As far as we recognize, this is the first report of the order-by-disorder process in fermionic system in a vdW coupled antiferromagnet, which opens various unique research directions for the future.

Methods

Synthesis of monocrystalline $\text{Ce}(\text{Se}_x\text{Te}_{1-x})\text{Te}_2$

Single crystals of $\text{Ce}(\text{Se}_x\text{Te}_{1-x})\text{Te}_2$ are grown using self-flux method. The mixture of the elemental powder of cerium (99.9%), selenium (99.999%), and tellurium (99.999%) in a molar ratio of 1 : $2x/3$: $40-2x/3$ was placed inside the alumina crucible and sealed in an evacuated quartz tube. The ampoule was heated to 900°C at a rate of 75°C/hour, kept at 900°C for 24 hours, and then slowly cooled down to 550°C at a rate of 2°C/hour followed by centrifugation to remove crystals from the melt.

Magnetization and heat capacity measurement

DC magnetization and heat capacity were measured using a Magnetic Property Measurement System (Quantum Design) with a ^3He insert⁴⁷ and a Physical Property Measurement System PPMS (Quantum Design) with a ^3He insert, respectively.

Estimation of magnetic heat capacity

We extracted the magnetic fluctuation strength from heat capacity $C(T)$ (**Fig. 3a-f left axis**) based on the method described as follows. To obtain the 4f electron contribution $C_f(T)$, first we subtract $C(T)$ of LaTe_3 from that of $\text{Ce}(\text{Se}_x\text{Te}_{1-x})\text{Te}_2$. This subtraction relies on the assumption that phonon and electronic contributions not arising from the 4f electrons are the same between LaTe_3 and $\text{Ce}(\text{Se}_x\text{Te}_{1-x})\text{Te}_2$ (see supplemental information). From comparison, the specific heat is dominated by 4f electron derived signal, and phonon subtraction is a minor correction within the main purpose of this study. Using the obtained $C_f(T)$, Here, we set $C_f(0)=0$ to calculate $S(T)$. This assumption is physically not exactly accurate since heat capacity is finite due to itinerant 4f-electron nature; It does not however have a large impact within the purpose of extracting magnetic entropy since electronic contribution relative to magnetic contribution is much lower.

Data availability

The datasets collected and analysis performed by this study are available from the corresponding author upon reasonable request.

Acknowledgements

The cell structure was visualized using VESTA⁴⁸. Heat capacity measurements were carried out under the Visiting Researcher's Program of Institute for Solid State Physics, The University of Tokyo. We thank S. Asai and S. Hasegawa for helping with heat capacity measurements.

Author contribution

Y. O. and R. K. conceived this project. D. U, S. K., Y. F., R. K., Y. O., B. S., Y. I., W. S., T. M., and T. K. corrected experimental data. C. H., H. L., and F. C., theoretically considered electronic structure. R. O. and Y. O. interpret the data. Y. O., R. O., and B. S. wrote the manuscript. We all discussed.

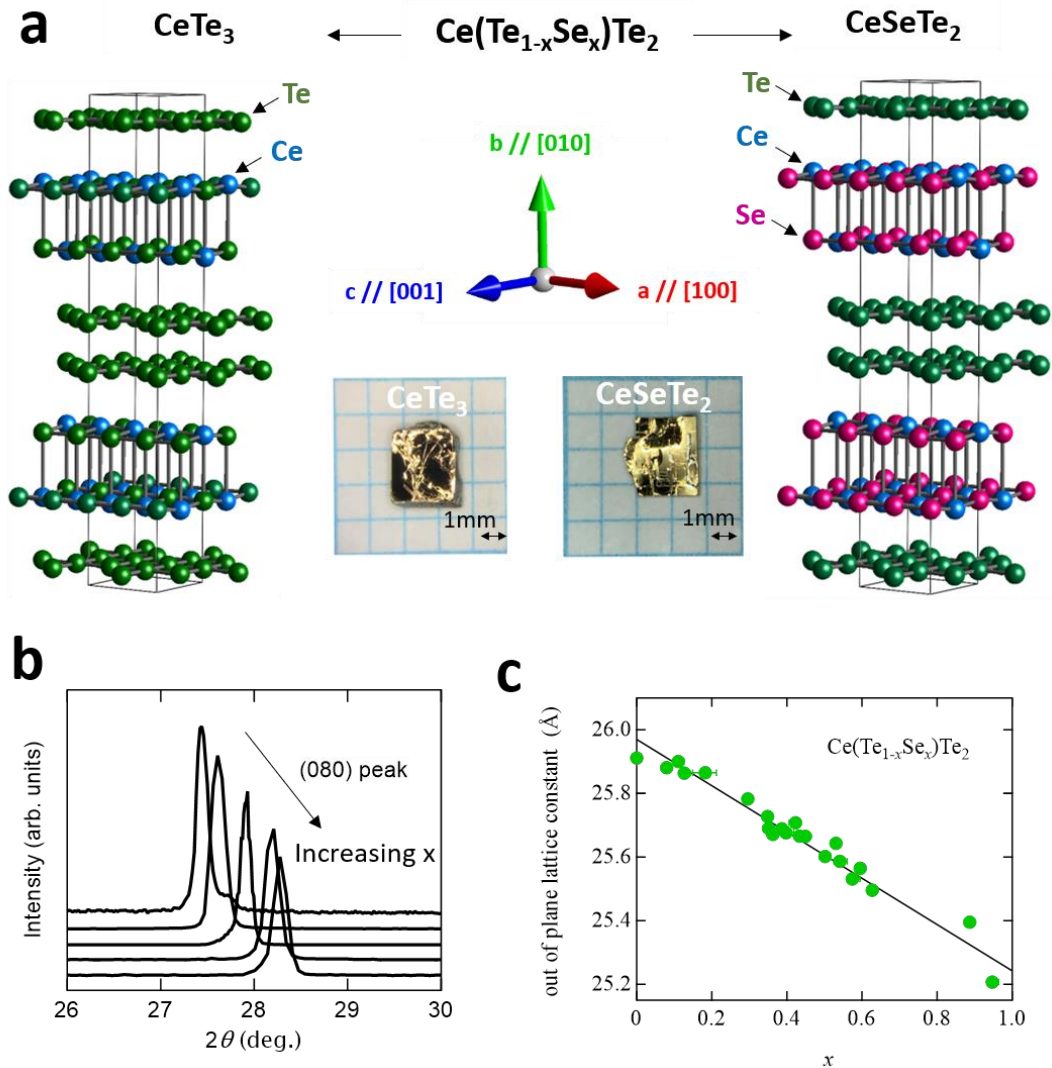


Fig. 1 Systematic change of chemical pressure by iso-valent elemental substitution in a vdW coupled material $\text{Ce}(\text{Se}_x\text{Te}_{1-x})\text{Te}_2$. (a) Crystal structures of CeTe_3 (left) and CeSeTe_2 (right). Substituted Se atoms enter the magnetic blocking layer selectively. The typical picture of single crystals and the definition of crystallographic directions are also shown. (b) Doping dependence of characteristic X-ray diffraction (XRD) patterns near the (0 8 0) peak for $\text{Ce}(\text{Se}_x\text{Te}_{1-x})\text{Te}_2$. (c) The out of plane lattice constant b as a function of doping x determined from energy dispersive X-ray spectrometry (EDX). This relation was obtained by performing both XRD and EDX on individual crystal flakes.

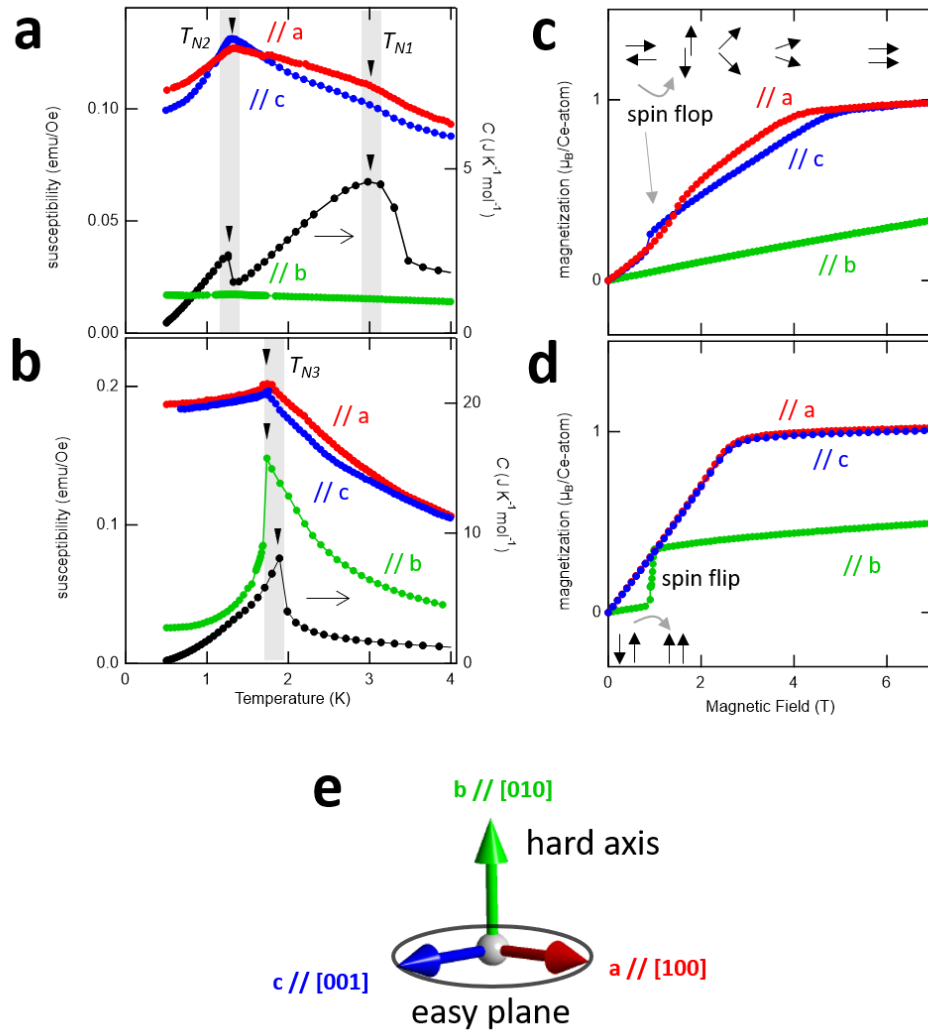


Fig. 2 Magnetism and heat capacity characterization for CeTe_3 and CeSeTe_2 samples. (a,b) Temperature dependence of the magnetic susceptibility (right axis) for (a) CeTe_3 and (b) CeSeTe_2 with applying external field $H = 0.1$ T. On the right axis, temperature dependence of the heat capacity $C(T)$ is also shown. In (a) and (b), there is slight difference in transition temperature since different samples were used for magnetic and heat capacity measurements. (c, d) Magnetic field dependence of the magnetization for (c) CeTe_3 and (d) CeSeTe_2 at $T = 0.5$ K. Cartoons for the magnetization process with spin-flop along easy plane and spin-flip along hard axis are shown in (c) and (d), respectively. The red, blue, and green data shown in (a)-(d) are obtained for $H // a$, $H // c$, and $H // b$, respectively. (e) The experimentally determined magnetic hard axis and easy plane together with crystal axes. These crystallographic and magnetic directions are the same for all samples shown in this study.

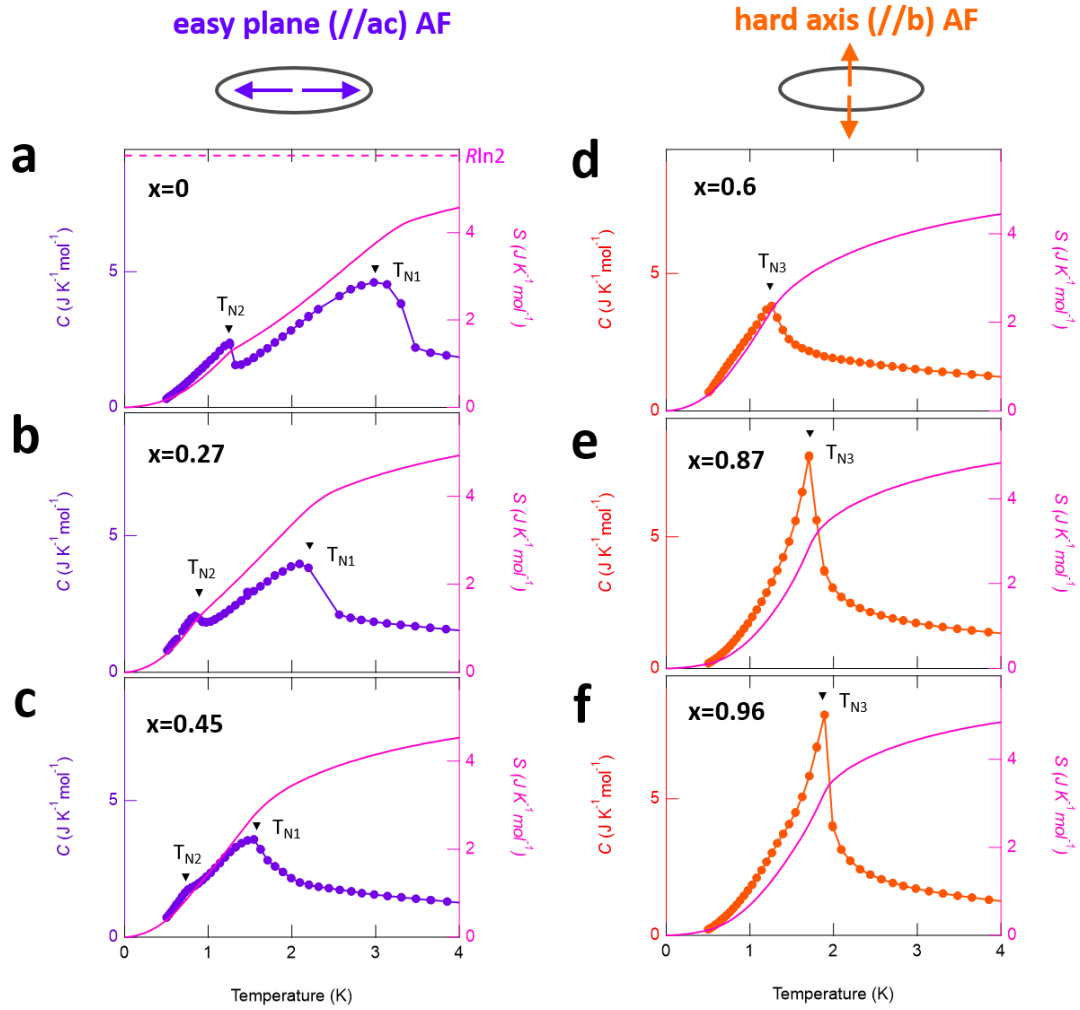


Figure 3 Doping and temperature dependence of heat capacity $C(T)$ of $\text{Ce}(\text{Se}_x\text{Te}_{1-x})\text{Te}_2$. (a-f) Temperature dependence of the heat capacity (circles; left axis) and magnetic entropy (solid line; right axis) of (a) $x=0$, (b) $x=0.27$, (c) $x=0.45$, (d) $x=0.60$, (e) $x=0.87$, (f) $x=0.96$. The purple color represents data obtained from samples with easy plane antiferromagnetism (AF), and the orange represents those with hard axis AF. In (a), the value $R\ln 2$ ($\sim 5.76 \text{ J K}^{-1} \text{ mol}^{-1}$) is shown with a broken line. This value is the calculated magnetic entropy from the ground state doublet of Ce^{3+} ions under the crystalline electric field.

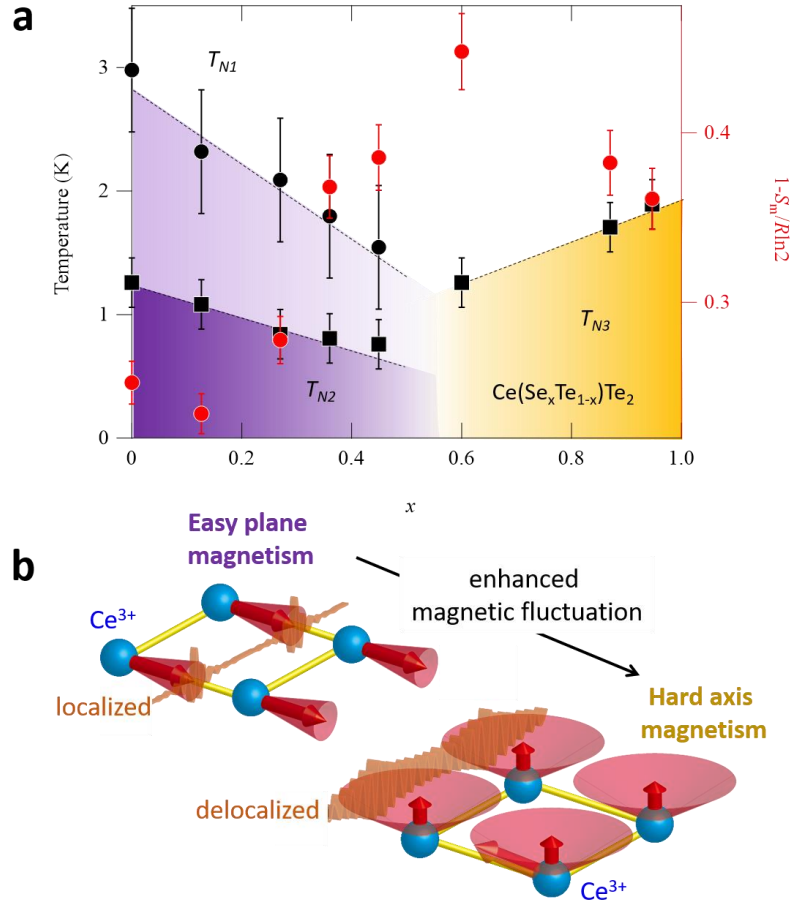


Figure 4 The phase diagram representing magnetic rotation associated with enhanced quantum fluctuation. **(a)** Temperature-doping phase diagram of $Ce(Se_xTe_{1-x})Te_2$ for three successive magnetic transition temperatures (T_{N1} , T_{N2} , and T_{N3}) and magnetic entropies $1-S_m/Rln2$. The data used in this phase diagram are from specific heat measurements. **(b)** Schematic drawing of Fermionic order by disorder. The magnetic moment lies in the easy axis (plane) and is reduced with enhanced quantum fluctuation for $x < 0.54$. Whereas with enhanced fluctuation the magnetic moment moves to lie along the hard axis ($x > 0.54$) and expresses enhanced precession as for an Ising-like moment. The kinetic energy gain with enhanced magnetic fluctuation is represented as a change from localized wave packet (left) to delocalized wave packet (right). As a detailed spin structure for antiferromagnetism within this compound is not totally clear, ferromagnetically aligned spins within single Ce square lattice sheet along ac plane (see Fig. 1a and Fig. 2a) are drawn for clarity.

References

- ¹ Keimer, B., Kivelson, S. A., Norman, M. R., Uchida, S. & Zaanen, J. From quantum matter to high-temperature superconductivity in copper oxides. *Nature* **518**, 179–186 (2015).
- ² Stewart, G. R. Superconductivity in Iron Compounds. *Rev. Mod. Phys.* **83**, 1589-1652 (2011).
- ³ Stewart, G. R., Heavy-fermion systems. *Rev. Mod. Phys.* **56**, 755 (1984).
- ⁴ Coleman, P. Heavy Fermions and the Kondo Lattice: a 21st Century Perspective. *arXiv:1509.05769*
- ⁵ Imada, M., Fujimori, A. & Tokura, Y. Metal-insulator transitions. *Rev. Mod. Phys.* **70**, 1039 (1998).
- ⁶ Masuda, H. *et al.* Quantum Hall effect in a bulk antiferromagnet EuMnBi_2 with magnetically confined two-dimensional Dirac fermions. *Sci. Adv.* **2**, 1501117 (2016).
- ⁷ Kida, T. *et al.* The giant anomalous Hall effect in the ferromagnet Fe_3Sn_2 —a frustrated kagome metal. *J. Phys.: Condens. Matter* **23**, 112205 (2011).
- ⁸ Nakatsuji, S., Kiyohara, N. & Higo, T. Large anomalous Hall effect in a non-collinear antiferromagnet at room temperature. *Nature* **527**, 212 (2015).
- ⁹ Liu, E. *et al.* Giant anomalous Hall effect in a ferromagnetic kagome-lattice semimetal. *Nature Physics* **14**, 1125 (2018).
- ¹⁰ Fang, Z. *et al.* The Anomalous Hall Effect and Magnetic Monopoles in Momentum Space. *Science* **302**, 92 (2003).
- ¹¹ Soumyanarayanan, A., Reyren, N., Fert A. & Panagopoulos, C. Emergent phenomena induced by spin–orbit coupling at surfaces and interfaces. *Nature* **539**, 509 (2016).
- ¹² Matsuno, J. *et al.* Interface-driven topological Hall effect in SrRuO_3 - SrIrO_3 bilayer. *Sci. Adv.* **2**, e1600304 (2016).
- ¹³ Soumyanarayanan, A. *et al.* Tunable Room Temperature Magnetic Skyrmions in Ir/Fe/Co/Pt Multilayers. *Nat. Mat.* **16**, 898-904 (2017).
- ¹⁴ Nagaosa, N. & Tokura, Y., Topological properties and dynamics of magnetic skyrmions. *Nat. Nanotech.* **8**, 899 (2013).

- ¹⁵ Geim, A. K. & Grigorieva, I. V. Van der Waals heterostructures. *Nature* **499**, 419 (2013).
- ¹⁶ Zhang, Y. *et al.* Emergence of Kondo lattice behavior in a van der Waals itinerant ferromagnet, Fe₃GeTe₂. *Sci. Adv.* **4**, eaao6791 (2018).
- ¹⁷ Fei, Z. *et al.* Two-dimensional itinerant ferromagnetism in atomically thin Fe₃GeTe₂. *Nat. Mater.* **17**, 778–782 (2018).
- ¹⁸ Kim, K. *et al.* Large anomalous Hall current induced by topological nodal lines in a ferromagnetic van der Waals semimetal. *Nat. Mater.* **17**, 794 (2018).
- ¹⁹ Deng, Y. *et al.* Gate-tunable room-temperature ferromagnetism in two-dimensional Fe₃GeTe₂. *Nature* **563**, 94 (2018).
- ²⁰ May, A. F. *et al.* Ferromagnetism Near Room Temperature in the Cleavable van der Waals Crystal Fe₅GeTe₂. *ACS Nano* **13**, 4436-4442 (2019).
- ²¹ Lei, S. *et al.* High mobility in a van der Waals layered antiferromagnetic metal. *Sci. Adv.* **6**, eaay6407 (2020).
- ²² Iyeyri, Y., Okumura, T., Michioka, C. & Suzuki, K. Magnetic properties of rare-earth metal tritellurides RTe₃ (R = Ce, Pr, Nd, Gd, Dy). *Phys. Rev. B* **67**, 144417 (2003).
- ²³ Deguchi, K., Okada, T., Chen, G. F., Ban, S., Aso, N. & Sato, N. K. Magnetic order of rare-earth tritelluride CeTe₃ at low temperature. *J. Phys.: Conf. Ser.* **150**, 042023 (2009).
- ²⁴ Ru, N. & Fisher, I. R. Thermodynamic and transport properties of YTe₃, LaTe₃, and CeTe₃. *Phys. Rev. B* **73**, 033101, (2006).
- ²⁵ Klemenz, S., Lei, S. & Schoop, L. M. Topological Semimetals in Square-Net Materials. *Annu. Rev. Mater. Res.* **49**, 185-206 (2019).
- ²⁶ Schmitt, F. *et al.* Transient Electronic Structure and Melting of a Charge Density Wave in TbTe₃. *Science* **321**, 1649 (2008).
- ²⁷ Brouet, V. *et al.* Fermi Surface Reconstruction in the CDW State of CeTe₃ Observed by Photoemission. *Phys. Rev. Lett.* **93**, 126405 (2004).
- ²⁸ Brouet, V. *et al.* ARPES Study of the Evolution of Band Structure and Charge Density Wave Properties in

RTe₃ for R = Y, La, Ce, Sm, Gd, Tb and Dy. *Phys. Rev. B* **77**, 235104 (2008).

²⁹ DiMasi, E., Aronson, M. C., Mansfield, J. F., Foran, B. & Lee, S. Chemical Pressure and charge-density waves in rare-earth tritellurides. *Phys. Rev. B* **52**, 14516 (1995).

³⁰ Ru, N. *et al.* Effect of chemical pressure on the charge density wave transition in rare-earth tritellurides RTe₃. *Phys. Rev. B* **77**, 035114 (2008).

³¹ Wang, P. P. *et al.* Anisotropic Transport and Magnetic Properties of Charge-Density-Wave Materials RSeTe₂ (R=La, Ce, Pr, Nd). *Chin. Phys. Lett.* **32**, 087101 (2015).

³² Polequin, B., Tsinde, F. & Doert, T. The ternary rare-earth polychalcogenides LaSeTe₂, CeSeTe₂, PrSeTe₂, NdSeTe₂, and SmSeTe₂: Syntheses, crystal structures, electronic properties, and charge-density-wave-transitions. *Solid State Sci.* **7**, 573–587 (2005).

³³ Doert, T. *et al.* LaSeTe₂–Temperature Dependent Structure Investigation and Electron Holography on a Charge-Density-Wave-Hosting Compound. *Chem. Eur. J.* **9**, 5865–5872 (2003).

³⁴ Okada, Y. Takeuchi, T., Baba, T., Shin, S. & Ikuta, H. Origin of the Anomalously Strong Influence of Out-of-Plane Disorder on High-T_c Superconductivity. *J. Phys. Soc. Jpn.* **77**, 074714 (2008).

³⁵ José, J. V., Kadanoff, L. P., Kirkpatrick, S. & Nelson, D. R. Renormalization, vortices, and symmetry-breaking perturbations in the two-dimensional planar model. *Phys. Rev. B* **16**, 1217 (1978).

³⁶ Krüger, F., Pedder, C. J. & Green, A. G. Fluctuation-Driven Magnetic Hard-Axis Ordering in Metallic Ferromagnets. *Phys. Rev. Lett.* **113**, 147001 (2014).

³⁷ Green, A. G., Conduit, G. & Kruger, F. Quantum Order-by-Disorder in Strongly Correlated Metal. *Annu. Rev. Condens. Matter Phys.* **9** 59–77 (2018).

³⁸ Henley, C. L. Ordering due to disorder in a frustrated vector antiferromagnet. *Phys. Rev. Lett.* **62**, 2056 (1989).

³⁹ Lausberg, S. *et al.* Doped YbRh₂Si₂: Not Only Ferromagnetic Correlations but Ferromagnetic Order. *Phys. Rev. Lett.* **110** 256402 (2013).

⁴⁰ Steppke, A. *et al.* Ferromagnetic Quantum Critical Point in the Heavy-Fermion Metal YbNi₄(P_{1-x}As_x). *Science* **339**, 933 (2013).

- ⁴¹ Ishida, K. *et al.* YbRh₂Si₂: Spin Fluctuations in the Vicinity of a Quantum Critical Point at Low Magnetic Field. *Phys. Rev. Lett.* **89**, 107202 (2002).
- ⁴² Klingner, C. *et al.* Evolution of magnetism in Yb(Rh_{1-x}Co_x)₂Si₂. *Phys. Rev. B* **83**, 144405 (2011).
- ⁴³ Andrade, E. C., Brando, M., Geibel, C. & Vojta, M. Competing orders, competing anisotropies, and multicriticality: The case of Co-doped YbRh₂Si₂. *Phys. Rev. B* **90**, 075138 (2014).
- ⁴⁴ Khalyavin, D. D., *et al.* Change of magnetic ground state by light electron doping in CeOs₂Al₁₀. *Phys. Rev. B* **88**, 060403(R) (2013).
- ⁴⁵ Bhattacharyya, A. *et al.* Anomalous change of the magnetic moment direction by hole doping in CeRu₂Al₁₀. *Phys. Rev. B* **90**, 174412 (2014).
- ⁴⁶ Watanabe, M. *et al.* Quantum oscillations with magnetic hysteresis observed in CeTe₃ thin films. APEX (submitted)
- ⁴⁷ Sato, Y. *et al.* Development of a low-temperature insert for precise magnetization measurement below $T = 2$ K with a superconducting quantum interference device magnetometer. *Jpn. J. Appl. Phys.* **52**, 106702 (2013).
- ⁴⁸ Momma, K. & Izumi, F. *J. Appl. Cryst.* **44**, 1272-1276 (2011).